



Preparation of Flexible Substrate Electrode for Supercapacitor With High-Performance MnO₂ Stalagmite Nanorod Arrays

Yuanyu Ge, Xianfeng Wang and Tao Zhao*

College of Chemistry, Chemical Engineering and Biotechnology, Donghua University, Shanghai, China

A large-area MnO₂ stalagmite nanorod arrays (SNAs) growing vertically on flexible substrates were successfully fabricated by an easy heat-electrodeposition method. The large specific capacitance (646.4 F g⁻¹ at 500 mA g⁻¹) and excellent rate capability (42.3% retention with 40 times of increase) indicate that the prepared MnO₂ SNAs flexible electrode has outstanding electrochemical performance. Furthermore, after 5,000 repetitions of CV tests, the overall specific capacitance could retain ~101.2% compared with the initial value meant a long cycling life. These outstanding properties could be ascribed to the effective conductive transport path between Ni substrate and MnO₂ nanorods, and owing to the stalagmite like structure of MnO₂ nanorods, the exposed sufficient active sites are beneficial to the electrolyte infiltration.

OPEN ACCESS

Edited by:

Wenyao Li,
Shanghai University of Engineering
Sciences, China

Reviewed by:

Bo Li,
Shanghai Jiao Tong University, China
Guangjin Wang,
Hubei Engineering University, China

*Correspondence:

Tao Zhao
tzhao@dhu.edu.cn

Specialty section:

This article was submitted to
Electrochemistry,
a section of the journal
Frontiers in Chemistry

Received: 09 April 2019

Accepted: 25 April 2019

Published: 14 May 2019

Citation:

Ge Y, Wang X and Zhao T (2019)
Preparation of Flexible Substrate
Electrode for Supercapacitor With
High-Performance MnO₂ Stalagmite
Nanorod Arrays. *Front. Chem.* 7:338.
doi: 10.3389/fchem.2019.00338

Keywords: large-area, manganese dioxide, stalagmite nanorod arrays, supercapacitors, flexible electrode

INTRODUCTION

The expanding requirement for energy consumption has stimulated the development of electrochemical energy storage devices (Simon and Gogotsi, 2008). Supercapacitors (SCs) occupy an important position in the field of energy storage devices due to their high power density, high-speed of charging and discharging and long cycle life (Burke, 2000). Nowadays, the development of supercapacitors to higher mechanical flexibility has become one of the important trends. It is shown that materials, such as graphene, transition metal dichalcogenides, MXenes (Han et al., 2018), and nanocellulose-graphene composites (Xing et al., 2019) could be used to construct nanomaterials-based flexible electrodes with high performance for supercapacitors, and there were relationships between structures and properties.

There are many different SCs electrode materials, such as carbon-based material (Li G. et al., 2018; Takeuchi et al., 2018) for the electric double layer capacitors (EDLCs), transition metal oxides, nitrides (Yi et al., 2018) and nickel based materials (Feng et al., 2014; Li et al., 2018) for the pseudocapacitors (PCs). Manganese dioxide (MnO₂) is one of the rapid developed metal oxide electrode materials in recent years (Wang et al., 2015). α -MnO₂ has a high specific capacitance among the various crystallographic structures of MnO₂, which is mainly due to its largest tunnel (Sanger et al., 2016) that can store more foreign cations for charge balance. More importantly, the electrolytes used for MnO₂ electrodes are non-corrosive neutral solutions, which is green and fit for environmental protection (Li et al., 2012).

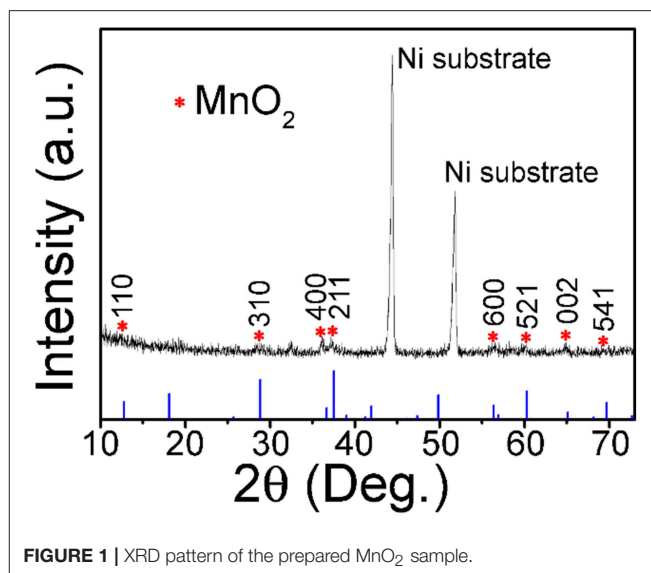
As we know, the effects of active materials on the performance of SCs include morphology, structure, contact with collector plate and active sites, etc. Unfortunately, during the redox reaction, the electrons transport of MnO₂ electrodes often restricted by its high electrical resistivity. In addition, the defect of the conventional powder electrode preparation is that the generated 'dead volume' by the bonding process of the active material to substrate could make a deterioration in the electrochemical properties of the electrodes (Liu et al., 2016). To solve the defects noted above, it could be a feasible way to manufacture binder-free MnO₂ supporting on 3D conductive substrates. The benefits of the 3D binder-free electrode are the enhanced electron transport and sufficient free space between the nanostructures, which contribute to the generation of more active sites for Faradaic reaction. Li et al. prepared the Ni foam-based ultrafine MnO₂ nanobelts with capacitance of 509 F g⁻¹ at 0.2 A g⁻¹ (Li et al., 2013). Davoglio et al. (2018) synthesized the α -MnO₂ particles at the aqueous-organic interface with capacitance of 289 F g⁻¹ at 0.5 A g⁻¹. Although some achievements have been made in the preparation of MnO₂ electrodes on conductive substrates, there is still great potential to develop easy methods for the preparation of high performance MnO₂ nanowires with various forms.

In this paper, the heat-electrodeposition method was adopted to formulate a nanoarrays of stalagmite like MnO₂ on the flexible substrates. The prepared electrode gets capacitance of 646.4 F g⁻¹ (500 mA g⁻¹) and 42.3% retention (current density increased 40 times) for a remarkable rate capability. And the total capacitance retention rate after 5,000 cycles is ~101.2%. Furthermore, to verify the generality of the synthesis method, another flexible activated carbon fiber (ACF) was also used as the substrate for the growth of MnO₂ nanoarrays.

EXPERIMENTAL

Material Preparation

The preparing method in detail was: the heat-electrodeposition process carried on a 3D porous Ni foam. Before electrodeposition, the Ni foam was cut into $\sim 3 \times 1 \text{ cm}^2$, and then immersed into a 5 mol/L HCl solutions along with supersonic wave treatment for 10 min to dissolve the NiO layer on the surface. The Ni foam obtained from the previous step was rinsed to neutral with distilled water, and then subjected to vacuum drying (60°C, 4 h). The heat-electrodeposition occurred in a cell with the water bath. The composition of the electrolyte was as follows: Mn(CH₃COO)₂ (0.01 M), CH₃COONH₄ (0.02 M) and dimethylsulfoxide (DMSO, 10 vol.%). The corresponding working electrode, the counter electrode and the reference electrode were the treated Ni foam, the Pt plate (1.5 × 1.5 cm²) and saturated calomel electrode (SCE), respectively. The heat-electrodeposition condition was applied at a constant current (0.5 mA cm⁻²) by the Autolab electrochemical workstation at $\sim 80^\circ\text{C}$ for 60 min. After that rinsed the obtained sample to neutral and placed it in a 60°C vacuum dryer for 4 h. Finally, the sample was calcined in N₂ atmosphere (heating-up 0.5°C min⁻¹, 250°C, 2 h). The weight gain of the sample after the deposition was the active matter weight.



Material Characterizations

In order to analyze the samples qualitatively, the X-ray diffractometer (XRD; Rigaku D/max-2550 PC, Cu-K α radiation) spectrum was utilized. To observe the microstructures, scanning electron microscope (SEM, Hitachi S-4800) and transmission electron microscope (TEM, JEOL JEM-2100F) were adopted. Mass weighing (Mettler Toledo XS105DU, $\delta = 0.01 \text{ mg}$).

Electrochemical Measurements

The Electrochemical Workstation (Autolab PGSTAT302N, electrolyte 0.5 M Na₂SO₄) was used to measure electrochemical performance. In the test, the obtained MnO₂ electrode ($\sim 1 \text{ cm}^2$) was used as the working electrode. The counter and reference electrode were the same as mentioned above. Specific capacitance calculation (Guan et al., 2017):

$$C = I \cdot \Delta t / (\Delta V \cdot m) \quad (1)$$

where C (F g⁻¹) is the specific capacitance, I (A) is the discharge current, Δt (s) is the discharge time consumed in the potential range of ΔV , ΔV (V) is the potential window, m (g) is the mass of the active materials.

The weight of the 1 cm² MnO₂ electrode was $\sim 1.32 \text{ mg}$. The cyclic voltammetry (CV) potential window was -0.1 to 0.9 V . The scan rates increased from 1 to 100 mV s⁻¹. The galvanostatic charge-discharge (GCD) curves were measured under current densities from 0.5 to 20 A g⁻¹. The cycle life was obtained by CV test (50 mV s⁻¹) with repetitions of 5,000.

RESULTS AND DISCUSSIONS

Except for the two strong peaks of 3D Ni foam substrate, the XRD diffraction pattern in **Figure 1** shows that other peaks at 12.8, 28.8, 36.7, 37.5, 56.4, 60.3, 65.1, and 69.7°, which are characteristic (110), (310), (400), (211), (600), (521), (002), and

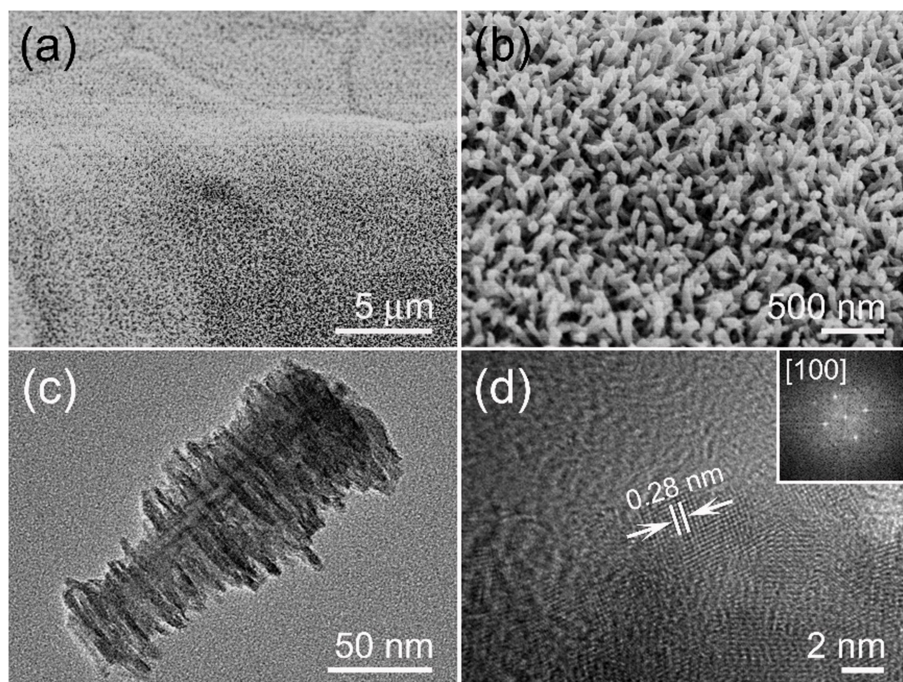


FIGURE 2 | (a) Low and (b) enlarged SEM photos of MnO₂ nanoarrays. (c) TEM image of the stalagmite MnO₂ nanorod. (d) Lattice resolved HRTEM image of a MnO₂ nanorod, an upper right inset showing its corresponding FFT pattern.

(541) reflections of α -MnO₂ (JCPDS 44-0141, $a = b = 9.785 \text{ \AA}$ and $c = 2.863 \text{ \AA}$), respectively.

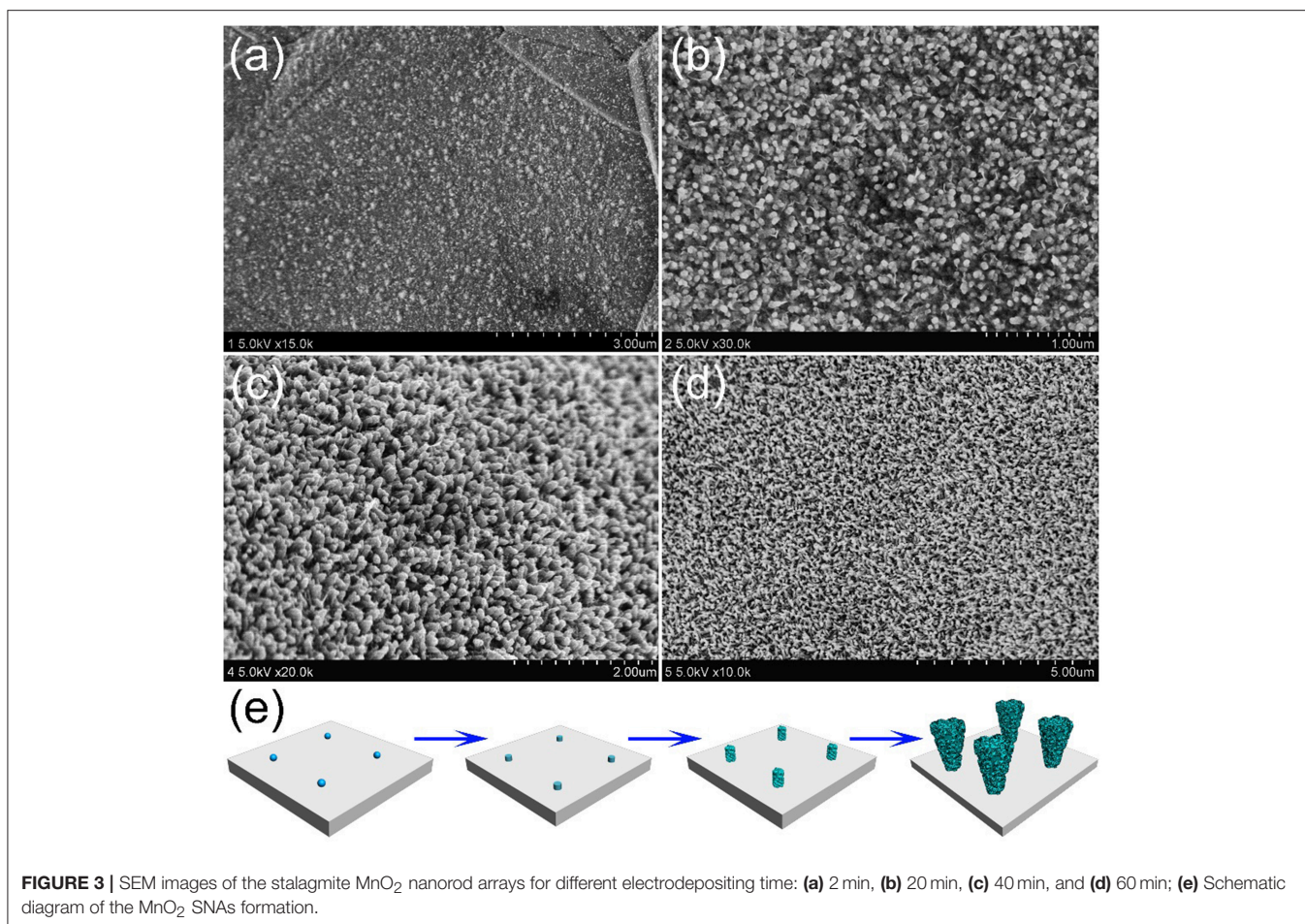
An aligned and dense MnO₂ nanoarray is presented in **Figure 2a** and there are no macroscopic defects among them. The enlarged SEM image of **Figure 2b** shows a highly open structure was formed by a vertical MnO₂ arrays on the substrate, which is conducive to the full entry of electrolytes. The TEM characterization was performed in order to get more structural information of the MnO₂ arrays. **Figure 2c** is a single stalagmite like MnO₂ nanorod which appears to be truncated cone-shaped with burrs on its surface. The typical diameters are $\sim 30 \text{ nm}$ of the root and $\sim 80 \text{ nm}$ of the top, and the length is up to $\sim 180 \text{ nm}$. HRTEM image of the single MnO₂ nanorod edge (**Figure 2d**) suggests that the surface is clearly with uniform single crystal and the interplanar spacing of 0.28 nm matches the (001) lattice plane of α -MnO₂ crystal. In addition, FFT diffraction pattern can also be associated with [100] zone axis of α -MnO₂ crystal (inset of **Figure 2d**).

In order to understand how the unique structure of stalagmite MnO₂ nanorod arrays (MnO₂ SNAs) was formed, the time-dependent electrodepositing experiments were carried out through controlling the electrodeposition reaction time. **Figure 3a** shows that after deposition of 2 min, nanoparticles can be seen on the surface of the substrate with the diameters of $10\text{--}20 \text{ nm}$. When the reaction time increases to 20 min, lots of well-distributed cylindrical nanorods began to appear, as displayed in **Figure 3b**. After doubling the reaction time, some irregular burrs were observed around the increased nanorods (**Figure 3c**). As shown in **Figure 3d**, after 60 min of

the electrodeposition, it is found that large-scale and uniform nanorod arrays were formed. The change of the morphology of the samples after different electrochemical deposition time could help us estimate the formation process of the MnO₂ nanorod arrays. In the early stage of the reaction, the formation of the nucleus in the precursor solution and the 1D growth behavior of Mn²⁺ (Ding et al., 2011) occurs successively, which result in the deposition of some tiny nanorods randomly and fast all over the surface. As the deposition intensifies, nanoparticles develop into nanorods with burrs, similar to stalagmite. When the reaction time reached to 1 h, the nanorods presented a truncated cone-shaped and formed a high-density array. The formation process of MnO₂ SNAs was elucidated in **Figure 3e**.

Furthermore, to verify the generality of the synthesis method, another flexible ACF substrate was chosen to replace the Ni foam. **Figure S1** shows that the dense needle-like MnO₂ nanorod arrays were grown on the ACF, which proves that the heat-electrodeposition method could be used to fabricate electrodes with different flexible substrates.

Figure 4A shows that the MnO₂ SNAs electrode CV with scanning rate from 1 to 100 mV s^{-1} were approximate to rectangle and symmetrical. All CV curves feature exhibits the pseudocapacitive nature (**Figure S3**) and a high-speed charge and discharge process (Hu et al., 2016). The possible reason for this phenomenon could be that the active sites in the microstructures of the stalagmite MnO₂ SNAs were fully in contact with electrolytes. The symmetrical GCD curves of the MnO₂ SNAs shown in **Figure 4B** revealed that the reversible redox reaction



and good electrochemical capacitance characteristics of the system. In addition, by comparing the specific capacitance of the Ni foam substrate and the prepared MnO₂ SNAs electrode in **Figure S2**, it is found that the substrate has little effect on the capacitance value.

In **Figure 4C**, the calculated specific capacitance of the electrode were 646.4, 587.1, 538.1, 463.6, 387.6, and 273.6 F g⁻¹ (Red Star), respectively, which were higher than reported works with similar MnO₂ structure (Li et al., 2013; Wang et al., 2017; Davoglio et al., 2018). **Figure 4C** also shows that the capacitance retention increased with the increase of current density. When it increased 40 times from 0.5 to 20 A g⁻¹, the corresponding specific capacitance reduced from 646.4 to 273.6 F g⁻¹ with the retention of 42.3%. The excellent rate capability indicates the potential of the MnO₂ SNAs electrode in high-power applications, and it could be caused by the unique open structure. The advantages of the open structure are that it is favorable for electrolyte infiltration and it owns large electrolytic accessible area, which not only promote redox reaction but also facilitates intercalation and de-intercalation of active species.

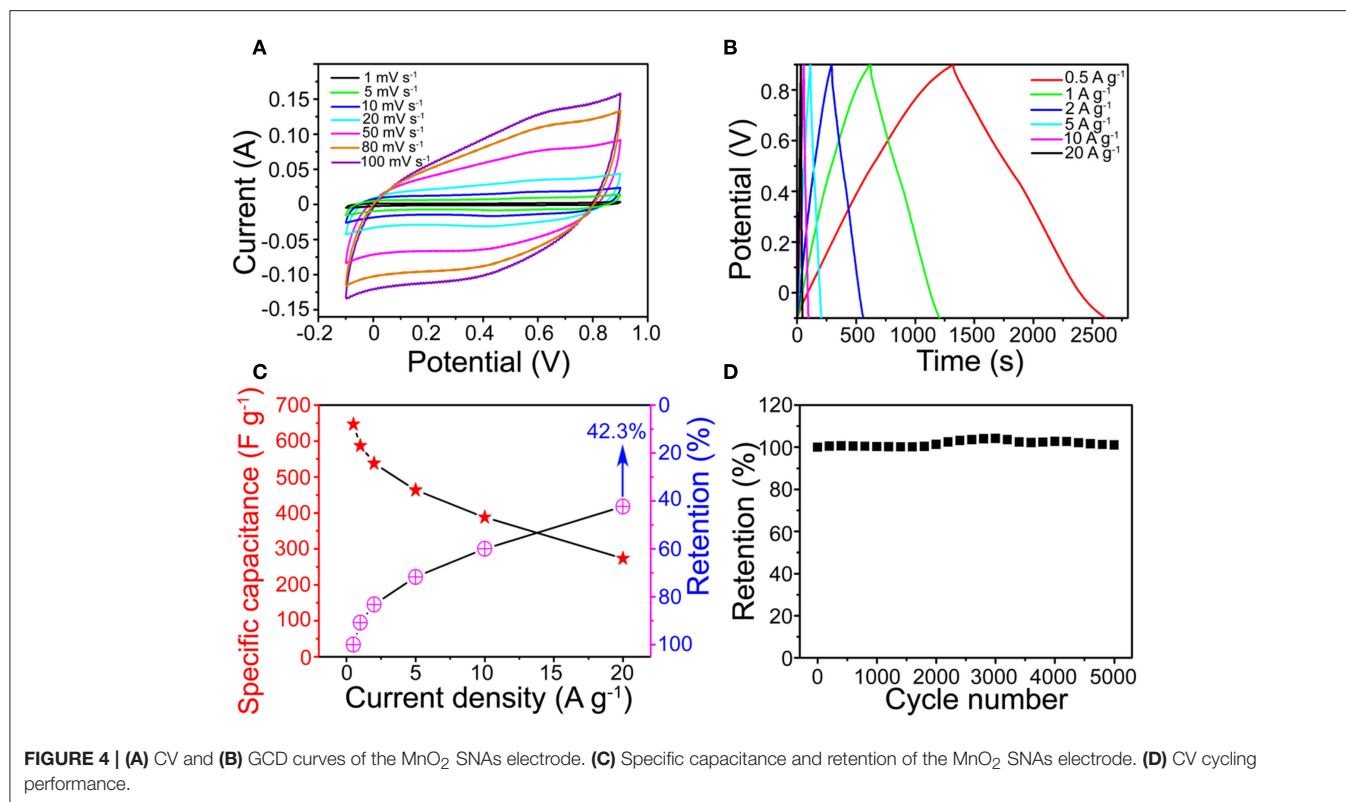
Figure 4D shows that a beneficial cycle life of the electrode and the capacitances retention enlarged during the initial 3,000 loops. The possible explanation is that the initially inactive part

of the MnO₂ SNAs electrode was activated by the permeated electrolyte and then the specific capacitance is increased (Xia et al., 2012).

After 5,000 cycles, a high specific capacitance retention of 101.2% indicated that the cyclical stability of the MnO₂ SNAs electrode was good. The strong contact between the active matters and the substrate facilitating the collection and enhancement of the electron participation reaction could be an important reason for the effective cycle stability. Thus, it is concluded that the electrode material of the as-synthesized MnO₂ SNAs demonstrates an excellent cycle life.

CONCLUSION

In conclusion, the stalagmite MnO₂ nanorod arrays successfully grew on the flexible substrate by heat-electrochemical deposition method. The prepared MnO₂ SNAs electrode has the high specific capacitance, the outstanding rate capability and the long cycle life, all of which all suggest its excellent electrochemical performance. In addition, this approach could pave the way for a facile low-temperature heat synthetic route for generating a variety of metal oxides arrays flexible substrate electrode.



DATA AVAILABILITY

The raw data supporting the conclusions of this manuscript will be made available by the authors, without undue reservation, to any qualified researcher.

AUTHOR CONTRIBUTIONS

YG did the experiments and described the images of figures. XW helping with writing. TZ was the supervisor of this research work. All authors participated in the analysis of experimental data and manuscript preparation.

REFERENCES

- Burke, A. (2000). Ultracapacitors: why, how, and where is the technology. *J. Power Sources* 91, 37–50. doi: 10.1016/S0378-7753(00)00485-7
- Davoglio, R. A., Cabello, G., Marco, J. F., and Biaggio, S. R. (2018). Synthesis and characterization of α -MnO₂ nanoneedles for electrochemical supercapacitors. *Electrochim. Acta* 261, 428–435. doi: 10.1016/j.electacta.2017.12.118
- Ding, S., Zhu, T., Chen, J. S., Wang, Z., Yuan, C., and Lou, X. W. (2011). Controlled synthesis of hierarchical NiO nanosheet hollow spheres with enhanced supercapacitive performance. *J. Mater. Chem.* 21, 6602–6606. doi: 10.1039/c1jm00017a
- Feng, L., Zhu, Y., Ding, H., and Ni, C. (2014). Recent progress in nickel based materials for high performance pseudocapacitor electrodes. *J. Power Sources* 267, 430–444. doi: 10.1016/j.jpowsour.2014.05.092
- Guan, B. Y., Yu, L., Wang, X., Song, S., and Lou, X. W. D. (2017). Formation of onion-like NiCo₂S₄ particles via sequential ion-exchange for hybrid supercapacitors. *Adv. Mater. Deerfield Beach Fla* 29:1605051. doi: 10.1002/adma.201605051
- Han, Y., Ge, Y., Chao, Y., Wang, C., and Wallace, G. G. (2018). Recent progress in 2D materials for flexible supercapacitors. *J. Energy Chem.* 27, 57–72. doi: 10.1016/j.jechem.2017.10.033
- Hu, J., Qian, F., Song, G., Li, W., and Wang, L. (2016). Ultrafine MnO₂ nanowire arrays grown on carbon fibers for high-performance supercapacitors. *Nanoscale Res. Lett.* 11:469. doi: 10.1186/s11671-016-1693-1
- Li, G., Gao, X., Wang, K., and Cheng, Z. (2018). Porous carbon nanospheres with high EDLC capacitance. *Diam. Relat. Mater.* 88, 12–17. doi: 10.1016/j.diamond.2018.06.010
- Li, W., Liu, Q., Sun, Y., Sun, J., Zou, R., Li, G., et al. (2012). MnO₂ ultralong nanowires with better electrical conductivity and enhanced supercapacitor performances. *J. Mater. Chem.* 22, 14864–14867. doi: 10.1039/c2jm33368f
- Li, W., Xu, K., An, L., Jiang, F., Zhou, X., Yang, J., et al. (2013). Effect of temperature on the performance of ultrafine MnO₂ nanobelt supercapacitors. *J. Mater. Chem. A* 2, 1443–1447. doi: 10.1039/C3TA14182A
- Li, W., Zhang, B., Lin, R., Ho-Kimura, S., He, G., Zhou, X., et al. (2018). A dendritic nickel cobalt sulfide nanostructure for alkaline battery electrodes. *Adv. Funct. Mater.* 28:1705937. doi: 10.1002/adfm.201705937

FUNDING

This work was supported by National Key R&D Program (2017YFB0309100) from Ministry of Science and Technology of the People's Republic of China.

SUPPLEMENTARY MATERIAL

The Supplementary Material for this article can be found online at: <https://www.frontiersin.org/articles/10.3389/fchem.2019.00338/full#supplementary-material>

- Liu, X., Chen, G., Guan, H., Dong, C., Xiao, X., and Wang, Y. (2016). Binder-free NiO@MnO₂ core-shell electrode: rod-like NiO core prepared through corrosion by oxalic acid and enhanced pseudocapacitance with sphere-like MnO₂ shell. *Electrochim. Acta* 189, 83–92. doi: 10.1016/j.electacta.2015.12.076
- Sanger, A., Kumar, A., Kumar, A., and Chandra, R. (2016). Highly sensitive and selective hydrogen gas sensor using sputtered grown Pd decorated MnO₂ nanowalls. *Sens. Actuators B Chem.* 234, 8–14. doi: 10.1016/j.snb.2016.04.152
- Simon, P., and Gogotsi, Y. (2008). Materials for electrochemical capacitors. *Nat. Mater.* 7, 845–854. doi: 10.1038/nmat2297
- Takeuchi, K., Fujishige, M., Ishida, N., Kunieda, Y., Kato, Y., Tanaka, Y., et al. (2018). High porous bio-nanocarbons prepared by carbonization and NaOH activation of polysaccharides for electrode material of EDLC. *J. Phys. Chem. Solids* 118, 137–143. doi: 10.1016/j.jpcs.2018.02.050
- Wang, J.-G., Kang, F., and Wei, B. (2015). Engineering of MnO₂-based nanocomposites for high-performance supercapacitors. *Prog. Mater. Sci.* 74, 51–124. doi: 10.1016/j.pmatsci.2015.04.003
- Wang, Y., Fu, A., Liu, X., Wang, Y., Li, Y., Guo, P., et al. (2017). Porous carbon directed growth of carbon modified MnO₂ porous spheres for pseudocapacitor applications. *J. Alloys Compd.* 717, 341–349. doi: 10.1016/j.jallcom.2017.05.035
- Xia, X., Tu, J., Zhang, Y., Wang, X., Gu, C., Zhao, X., et al. (2012). High-quality metal oxide core/shell nanowire arrays on conductive substrates for electrochemical energy storage. *ACS Nano* 6, 5531–5538. doi: 10.1021/nn301454q
- Xing, J., Tao, P., Wu, Z., Xing, C., Liao, X., and Nie, S. (2019). Nanocellulose-graphene composites: a promising nanomaterial for flexible supercapacitors. *Carbohydr. Polym.* 207, 447–459. doi: 10.1016/j.carbpol.2018.12.010
- Yi, C., Zou, J., Yang, H., and Leng, X. (2018). Recent advances in pseudocapacitor electrode materials: transition metal oxides and nitrides. *Trans. Nonferrous Met. Soc.* 28, 1980–2001. doi: 10.1016/S1003-6326(18)64843-5

Conflict of Interest Statement: The authors declare that the research was conducted in the absence of any commercial or financial relationships that could be construed as a potential conflict of interest.

Copyright © 2019 Ge, Wang and Zhao. This is an open-access article distributed under the terms of the Creative Commons Attribution License (CC BY). The use, distribution or reproduction in other forums is permitted, provided the original author(s) and the copyright owner(s) are credited and that the original publication in this journal is cited, in accordance with accepted academic practice. No use, distribution or reproduction is permitted which does not comply with these terms.